

# Cellular Network Densification: a System-level Analysis with IAB, NCR and RIS

Gabriel C. M. da Silva, *Student Member, IEEE*, Victor F. Monteiro, *Member, IEEE*, Diego A. Sousa, Darlan C. Moreira, Tarcisio F. Maciel *Senior Member, IEEE*, Fco. Rafael M. Lima, *Senior Member, IEEE* and Behrooz Makki, *Senior Member, IEEE*

**Abstract**—As the number of user equipments increases in fifth generation (5G) and beyond, it is desired to densify the cellular network with auxiliary nodes assisting the base stations. Examples of these nodes are integrated access and backhaul (IAB) nodes, network-controlled repeaters (NCRs) and reconfigurable intelligent surfaces (RISs). In this context, this work presents a system level overview of these three nodes. Moreover, this work evaluates through simulations the impact of network planning aiming at enhancing the performance of a network used to cover an outdoor sport event. We show that, in the considered scenario, in general, IAB nodes provide an improved signal to interference-plus-noise ratio and throughput, compared to NCRs and RISs. However, there are situations where NCR outperforms IAB due to higher level of interference caused by the latter. Finally, we show that the deployment of these nodes in unmanned aerial vehicles (UAVs) also achieves performance gains due to their aerial mobility. However, UAV constraints related to aerial deployment may prevent these nodes from reaching results as good as the ones achieved by their stationary deployment.

**Index Terms**—IAB, NCR, RIS, UAV, 5G, network densification.

## I. INTRODUCTION

The increasing number of connected devices and data traffic is pushing the boundaries of current wireless networks. By late 2029, data traffic is projected to reach 563 exabytes per month [1], up from 160 exabytes [1] at the end of 2023, marking a 3.5-fold increase. This surge is driven by innovations such as virtual and augmented reality, autonomous vehicles, and holographic projections. To accommodate this growth, fifth generation (5G) networks have moved beyond the congested sub-6 GHz spectrum (FR1) to include frequencies in the spectrum of millimeter waves (mmWaves) (FR2) [2]. While FR2 offers larger bandwidth [3], it faces challenges such as significant path loss and difficulty penetrating obstacles [4], [5]. Network densification with strategically placed nodes is used as a solution to extend coverage and enhance capacity.

The primary solution to densify the network is to deploy more next generation nodes B (gNBs) with fiber-based

Behrooz Makki is with Ericsson Research, Sweden. The other authors are with the Wireless Telecommunications Research Group (GTEL), Federal University of Ceará (UFC), Fortaleza, Ceará, Brazil. Diego A. Sousa is also with Federal Institute of Education, Science, and Technology of Ceará (IFCE), Paracuru, Brazil. This work was supported by Ericsson Research, Sweden, and Ericsson Innovation Center, Brazil, under UFC.51 Technical Cooperation Contract Ericsson/UFC. The work of Victor F. Monteiro was supported by CNPq under Grant 308267/2022-2. The work of Tarcisio F. Maciel was supported by CNPq under Grant 312471/2021-1. The work of Francisco R. M. Lima was supported by FUNCAP (edital BPI) under Grant BP5-0197-00194.01.00/22.

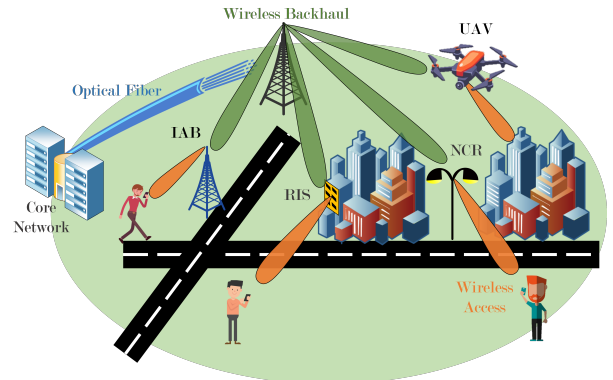


Fig. 1: Illustrative scenario with IAB node, NCR and RIS.

backhaul. However, building from scratch an entire new wired backhaul infrastructure might not be economically viable. Besides, it takes time, and, in certain locations such as historical areas, trenching may be prohibited [6]. In this context, wireless backhaul and technologies that increase the access extension have been considered as viable complementary solutions for achieving network densification.

Using relays for wireless backhaul is not a new concept. It was explored in 3rd generation partnership project (3GPP) long term evolution (LTE) Release 10 with LTE relays, but lacked commercial traction [7]. Other technologies, such as satellite and microwave point-to-point (PtP)/point-to-multi-point (PtmP), also use wireless backhaul [8]. Despite its history, wireless backhaul now garners increased commercial interest due to its proved ability to achieve over 100 Gbps [9] and its flexibility and cost-effectiveness [10]. Currently, a node with wireless backhaul under consideration is integrated access and backhaul (IAB) nodes, and nodes which enhance the access extension are network-controlled repeaters (NCRs) and reconfigurable intelligent surfaces (RISs) [3]. Figure 1 illustrates a scenario featuring these nodes.

IAB is a multi-hop setup where the same hardware and/or spectrum is used for both backhauling and access communication to the user equipments (UEs). This means that both access and backhaul links are wireless. IAB nodes began to be standardized by 3GPP in Release 16 [11], which addressed possible architectures, radio protocols, and physical layer aspects. Notably, access and backhaul links can be either in-band, sharing the same frequency spectrum, or out-of-band, using separate frequency bands.

Concerning NCRs, they were introduced by 3GPP in Release 18 [12]. NCRs can be seen as an enhancement of traditional radio frequency (RF) repeaters. One of the key differences between an NCR and a traditional RF repeater is that an NCR has beamforming capability controlled by a serving gNB via a side control link [12]. Furthermore, unlike a RF repeater, NCR is fully aware of the downlink (DL)/uplink (UL) split in the time division duplex (TDD) scheme, and is under the control of its controlling gNB which provides the NCR with side information [13].

With respect to RISs, they are made up of multiple antenna patches that use passive elements to introduce phase shifts to incoming signals [14], [15]. More specifically, they are composed of a metamaterial layer controlled by a gNB. Specifically, the metamaterial is a surface consisting of reflecting elements with electrical thickness in the order of subwavelength of the signal to which it is designed to work with. This allows for programmable control of the wireless environment [16].

To improve the performance of such nodes, a line of sight (LOS) link is recommended. This challenge should be managed during deployment, but achieving LOS between a serving gNB and an IAB/NCR/RIS can be difficult in certain situations, such as in urban areas with tall buildings. One temporary solution to overcome this problem is to mount these nodes on unmanned aerial vehicles (UAVs), which also offer mobility. It is important to note that, while 3GPP has standardized both stationary and mobile IAB nodes, NCRs are only standardized for stationary use, and RIS lacks standardization.

Few studies simultaneously address these three types of nodes. In [3], the authors refer to the environment where these technologies coexist as a heterogeneous smart electromagnetic environment. They provide an overview of each node, their industrial progress and their standardization status. However, they do not provide simulation results comparing the nodes' performances. They evaluate only the RIS performance. Another work addressing these nodes is [17]. The authors review each technology, discuss the 3GPP standardization status of IAB and NCR, and present reports from the European Telecommunications Standards Institute (ETSI) on RIS. However, as [3], [17] lacks simulation results comparing these nodes. Furthermore, system-level analyses are crucial. The presence of multiple of such nodes might have resource allocation and interference issues which can not be captured in link-level analyses, as presented in other works.

In this paper, we provide an overview of IAB, NCR and RIS. We discuss their main characteristics, e.g., architecture and specific features. Furthermore, we address different levels of mobility supported by them, including the possibility of deployment on UAVs. In this context, a brief overview of UAVs as serving nodes is also presented. A literature review of related research topics is provided for each node. We also analyze in a system-level perspective the impact of deploying these nodes in the environment. Simulation results are presented to assess the performance of these nodes when deployed either as stationary nodes or mounted on mobile UAVs.

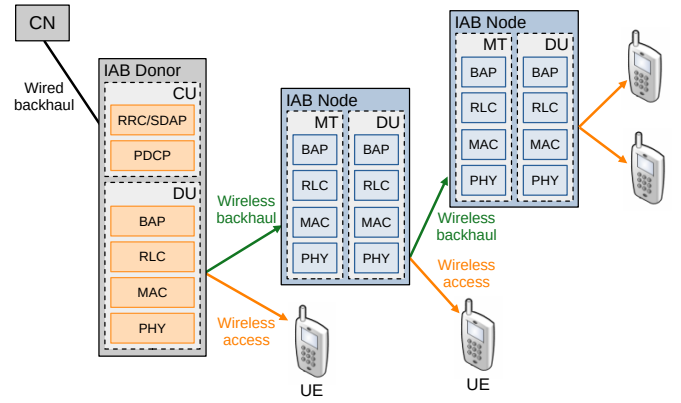


Fig. 2: Network with IAB nodes.

The present work is organized as follows. First, Section II provides a conceptual overview of IAB, NCR, RIS and UAV, including their architectural details and a literature review. Next, Section III introduces a system level model allowing a performance evaluation of these nodes. Based on the presented model and 3GPP standardized procedures, Section IV presents simulation results to assess the impact of deploying these nodes on system performance. An extensive performance analysis is then presented. Finally, Section V summarizes the conclusions of the work.

## II. EMERGING WIRELESS NETWORK NODES USED TO SERVE UES

### A. Integrated Access and Backhaul

The standardization of IAB by 3GPP started as a study item (SI) of 3GPP Release 15 in 2017. In Release 16, a technical report (TR) [11] published in 2018 detailed IAB system level aspects, e.g., topology management for single/multi-hop and redundant connectivity, route selection and dynamic resource allocation between the access and backhaul links. Later on, in 2020, Release 16 also started specifying IAB on two technical specifications (TSs): TS 38.300 [2], specifying protocol layers and architecture of IAB, and TS 38.174 [18], presenting the minimum RF characteristics and minimum performance requirements of IAB. In 2021, it was created, in Release 17, a work item entitled “Enhancements to IAB for NR” [19]. The main enhancements were related to: 1) duplexing (IAB was constrained to half duplex (HD) mode in Release 16, but it envisioned to support full duplex (FD) mode); 2) topology adaptation (procedures for inter-donor IAB node migration to enhance robustness and load balancing); and 3) routing and transport (improve multi-hop latency and congestion mitigation).

Figure 2 illustrates a network where some of the serving nodes have a wireless backhaul. The serving nodes in a system with IAB can be classified into two types: IAB donor and IAB node. The IAB donor is connected to the core network (CN) by a non-IAB, e.g., fiber backhaul, while the IAB nodes are connected to the IAB donor or another IAB node by a wireless IAB-based backhaul. The UEs, depicted as mobile phones, can be served by both IAB node types.

IAB donor can be split in two parts transparent to the served nodes [2]: centralized unit (CU) and distributed unit (DU). As in a regular gNB, on the one hand, the CU is responsible for less time-critical radio functionalities. On the other hand, the DU part is responsible for time-critical radio functionalities, e.g., scheduling and retransmission. This split is related to the possibility of deploying both parts in different geographical locations. For example, the DU may be close to the served nodes, in order to reduce communication delay, and the CU may be in a place with higher processing capability. Regarding their protocols, DU is responsible for lower layers, e.g., physical (PHY), medium access control (MAC) and radio link control (RLC); while CU is responsible for higher layers, e.g., packet data convergence protocol (PDCP) and radio resource control (RRC)/service data adaptation protocol (SDAP).

Regarding the IAB node, it is split in DU and mobile termination (MT). From a UE perspective, the DU acts as a regular gNB. From the perspective of an IAB donor, the MT acts as a regular UE.

To handle the traffic between an IAB donor and multiple IAB nodes, it was introduced a new sublayer called backhaul adaptation protocol (BAP) [20]. The IAB donor configures each IAB node with a unique BAP identification (ID) and a routing table that indicates its parent and possible children.

Taking into account the presented technical features of IAB, many works have already investigated different aspects related to this topic. In the following, we present some of them.

An important aspect usually addressed is the impact of IAB node position in the system performance. Some of the works that have evaluated this point are [21]–[23].

In [21], the authors consider a scenario where UEs are distributed in the coverage area of small and macro base stations (BSs). The backhaul link of the small BSs can be via fiber or wireless (in that case, it is an IAB node). Furthermore, the IAB network is submitted to blockage, tree foliage and rain. The authors conclude that it is necessary to have more IAB nodes than fiber-connected gNBs to achieve similar performance (in terms of UEs minimum required rate).

In [22] and [23], genetic algorithms (GAs) are utilized to place IAB nodes. The authors from [22] consider a scenario with temporary blockages and optimize via GA the IAB position to increase the service coverage probability. In [23], the authors study the cost-benefit between a scenario with only macro BSs and another with IAB nodes.

Another topic related to IAB systems is topology adaptation/routing, addressed in [24]–[26]. The authors of [24] compare two types of path selection policies, i.e., highest-quality-first and wired-first. The highest-quality-first policy chooses as parent node the candidate BS with the highest signal to noise ratio (SNR), while the wired-first policy prefers choosing a fiber-connected BS, i.e., an IAB donor, instead of another IAB node, even if the IAB donor provides a channel link worse than the one provided by another IAB node. The paper shows that, in the considered scenario, the wired-first policy outperforms the other strategy in terms of latency due a reduced number of intermediary nodes.

In [25] and [26], the authors propose algorithms for topology adaptation and routing aiming at load balancing.

In [25], the proposed solution is based on packet queue's length and uses graph theory to optimize the IAB network. The proposed algorithm increases the average throughput and the percentage of satisfied UEs. In [26], the algorithm aims at optimizing the trade-off between spectral efficiency and load balancing. In heavy data loading, the proposed solution outperforms benchmark solutions in terms of system rate. For light data loading, all solutions have similar results.

A third topic usually addressed by IAB works is the in-band resource allocation of access and backhaul links. Examples of works on this topic include [27]–[29].

In [27], the authors formulate a problem of spectrum resource allocation aiming at maximizing the sum log-rate of all UE. Due to the challenge of finding a solution for a mixed integer nonlinear programming (MINLP) problem, they propose a deep reinforcement learning method to reach real-time spectrum allocation satisfying the system requirements.

In [28], the authors' goal is to maximize the rate of the UEs. For this, they propose optimal and suboptimal algorithms to multiplex the UEs in frequency and space. They consider a power constraint scenario.

The objective of [29] is to simultaneously solve three problems where the scenario has mobile IAB nodes. The problems are: 1) define IAB nodes positions; 2) define UE-IAB association; 3) in-band resource allocation of backhaul and access links. To solve them, the authors propose a two-level hierarchical multi-agent learning, i.e., a type of reinforcement learning (RL).

## B. Network Controlled Repeater

In previous generations of wireless cellular networks, e.g., the fourth generation (4G), RF repeaters were used to enhance network coverage. They work as amplify and forward (AF) relays, introducing negligible latency, since they neither decode nor process the forwarded signal. Moreover, they are cost-effective and easy to deploy. However, they forward unwanted interference signals due to their lack of signal processing capability [12], [13], and they do not perform adaptive beamforming towards UEs which is required specially in FR2 [30].

NCR is an evolution of the traditional RF repeater. It was standardized in 3GPP Release 18. It can be controlled by the network via side control link, which enables, for example, an NCR to operate with spatial diversity via beamforming controlled by the network [12], [31].

Besides the fact that NCRs operate as AF repeaters, while IAB nodes operate as decode and forward (DF) relays, there are other differences between them. For example, on the one hand, NCR was standardized to be deployed as a stationary single-hop node. On the other hand, IAB can operate as a mobile node in a multi-hop deployment. The NCR is fully controlled by its controlling gNB, while the IAB node can make decisions on its own. Furthermore, IAB is more expensive than NCR.

An NCR can be split into two functional entities, i.e., NCR-MT and NCR-forwarding (Fwd), as shown in Fig. 3. The

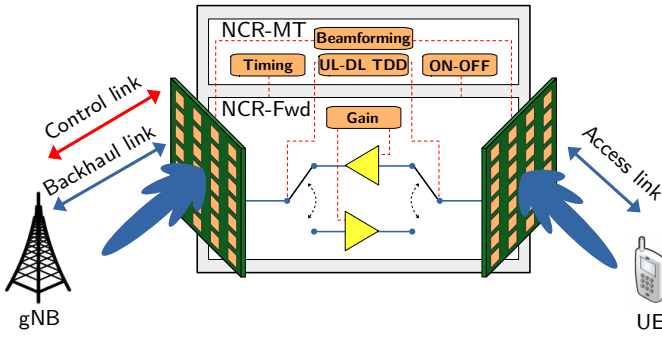


Fig. 3: NCR architecture.

NCR-MT entity is used to communicate with its controller gNB through a control link (C-link). The side control information controls the actions of NCR-Fwd. Regarding the NCR-Fwd, it is responsible for amplifying and forwarding the RF signals between a gNB and its serving UEs [32].

A common NCR deployment consists of having at least two antenna arrays, where one is responsible for receiving/transmitting control and backhaul links, and another is responsible for the access links.

Some of the information that can be exchanged through the C-link are [17]:

- *Beamforming information:* Traditional RF repeaters transmit omnidirectionally, causing interference and providing less power to target UEs. In contrast, NCR utilizes adaptive beamforming to address severe losses in mmWave, with the beamforming configuration managed by the controller gNB through C-link.
- *Timing information:* gNB can configure the temporal alignment between NCR reception and transmission for DL and UL. Specifically, a gNB may configure an NCR to introduce a delay in communication to prevent issues like interference between sequential transmissions.
- *Information on UL-DL TDD configuration:* C-link is also used to configure the NCR with a TDD scheme. NCR supports semi-static TDD DL/UL for access, backhaul, and control links to reduce the signaling. The DL/UL TDD configuration is the same for access and backhaul links [31].
- *ON-OFF information:* This information is sent to NCR for turning on/off the NCR-Fwd part. The main goals of this functionality is to save power and to mitigate potential interference caused by an NCR. The default mode is OFF. It stays in this state until a different gNB indication [12].

State-of-the-art works cover different aspects of NCR. In [31], the authors provide an overview on NCR. They present general aspects of side control information and discuss mechanisms for NCR identification and authentication. They compare three deployments: 1) macro only; 2) macro + RF repeater; and 3) macro + NCR. They also evaluate the impact of beamforming information on NCR's performance.

The authors of [33] discuss NCRs' main specifications in 3GPP Release 18 and the challenges associated with NCR-assisted networks, such as the lack of testbeds and cost-efficiency trade-offs between IAB and NCR. Their

simulation results suggest that deploying NCR can enhance performance particularly for UL and cell-edge UEs.

In [34]–[36], the authors compare NCR and RIS. Work [34] formulates mixed integer linear problems to maximize network reliability based on NCR and RIS positions and configurations. Study [35] focuses on physical layer and compares NCR and RIS coverage. It concludes that RIS is preferable for open areas despite its lower capacity, while NCR is better for narrow scenarios, e.g., roads. The authors of [36] evaluate NCR with and without power constraints and RIS with two beamforming algorithms, including hardware impairments. They conclude that, in general, NCR outperforms RIS, with RIS suffering the most when hardware impairments are present.

The authors of [37] evaluate an NCR with two panels for the access link. They aim to optimize a multi-user precoder to maximize the number of served UEs, considering constraints on the number of time-frequency resources and on the minimum required rate per UE. Compared with NCRs with only one antenna array in the access, two panels doubled the spectral efficiency (SE) and the number of served UEs.

In [38], the authors study the problem of beam squinting in NCR from link and system level perspectives. They consider signaling (i.e., control plane (CP)) and data (i.e., user plane (UP)) transmissions in different subbands. They propose a compensation method to prevent beam squinting caused by the configuration of the NCR to transmit data (UP) in a given subband based on measurements (CP) performed in another subband. The results show that, with their proposal, the NCR performs as good as if CP and UP shared the same subbands.

In [39], the authors analyze the interference impact of the NCR in a neighbor cell. They conclude that the interference can be mitigated by the choice of the beam that is used to serve the UEs. Besides, placing an NCR closer to the serving UE is not necessarily the position that maximizes the served UE performance nor the one that most harms a neighbor cell.

### C. Reconfigurable Intelligent Surface

Regarding 3GPP work on RIS, up to this moment, it has not started an SI on this topic. There was an expectation that an SI would be discussed in Releases 18 and 19, however it was not confirmed. Concerning the ETSI, in 2023, a group report (GR) was formulated to deliberate about several aspects related to RISs, e.g., deployment scenarios, architectures, and communication model [14], [40], [41].

RIS can dynamically or semi-statically alter electromagnetic (EM) properties of an incident wave. It consists of a thin metamaterial layer typically controlled by a gNB. This allows control over reflection, refraction, absorption and backscattering effects [14], enabling the creation of LOS links. The metamaterial surface has tunable properties, electronically adjusted by devices like positive-intrinsic-negatives (PINs) or varactor diodes [16]. A RIS standalone deployment is also envisioned with an integrated controller. A RIS transforms the wireless environment from a passive entity into a programmable intelligent agent [14].

A gNB manages the RIS by collecting data from the RIS and the UEs to estimate their channels and compute optimal

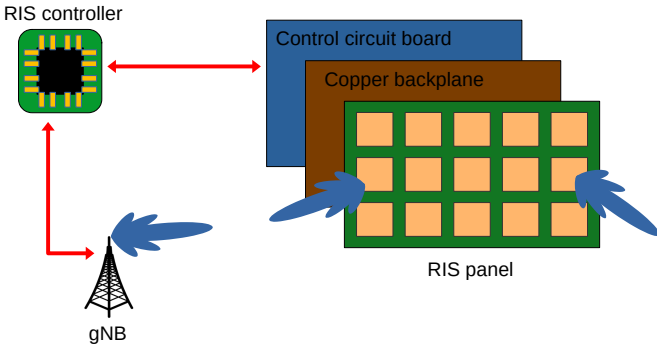


Fig. 4: RIS architecture.

beamforming. The gNB then configures the RIS to adjust its properties to improve system performance. Notably, the gNB handles all data processing, while the RIS merely implements the instructions received, which reduces production costs by eliminating the need for an internal processing unit.

As shown in Fig. 4, a RIS is composed of two main components: the RIS controller and the RIS panel. The RIS controller adjusts the properties of the unit cells to manipulate incoming EM waves based on gNB control signals. The panel is structured in multiple layers, with a simple model featuring three layers. The inner layer contains a control circuit connected to the RIS controller, which powers the circuit and manages its response. The middle layer, typically made of copper, serves as a shield to prevent signal leakage. The outermost layer consists of metallic unit cells that interact with the incident EM waves modifying its properties, e.g., amplitude, phase, and polarization [40].

RIS research spans various areas, with early studies focusing on channel estimation, as explored in [42]–[45]. In [42], researchers explore a communication system aided by RIS, considering physical imperfections, e.g., hardware-induced phase shift variations. They propose two tensor-based channel estimation algorithms using parallel factor analysis and evaluate their computational complexity.

The authors of [43] identify two key limitations in existing channel estimation algorithms: 1) rapid increase in computational complexity with more RIS elements, and 2) reliance on specific matrix structures. They propose an algorithm based on unitary approximate message passing, which scales linearly with the number of RIS elements and does not depend on specific matrix structures.

The authors of [45] consider a RIS-assisted system and propose a channel estimation method using convolutional neural network and autoregressive predictors. Compared to their benchmark, they achieve high prediction accuracy, improved spectral efficiency, and reduced pilot overhead.

RIS channel modeling is addressed in [46]–[49]. In [46], it is formulated a closed-form expression for free-space path loss models. Some aspects that are analyzed are the far-field and near-field beamforming. To validate their theoretical findings, they present measurements performed during an experiment in an anechoic chamber with three RISs. In [47] and [48], RISs are deployed in mobile UAVs. Both works study the channel statistics in the considered scenario. In [49], it is introduced

a method for calculating the scattered electric field generated by a RIS considering the mutual coupling of the unit-cells.

Beam design and selection is another well-researched area related to RIS-assisted networks, with notable works including [50]–[52]. Paper [50] surveys beamforming design, identifies research gaps, and suggests future research directions. Work [51] proposes a low-complexity adaptive beam selection scheme. It involves using two sub-optimal beamforming vectors, calculating the RIS beamforming, and selecting the solution that maximizes received signal strength. In [52], the authors consider the problem of maximizing the sum-rate of all UEs. They propose two solutions: a three-step convex optimization and a neural network scheme.

It is important to highlight that RIS is a huge area and the present work does not have the intention to cover all the topics. Other areas that can be mentioned are simultaneously transmitting and reflecting RIS [53], liquid-crystal RIS [54] and beyond diagonal RIS [55].

#### D. Unmanned Aerial Vehicle

In recent years, UAV applications have expanded into various fields, including delivery services, rescue, surveillance, military operations, and telecommunications [56]. This increased interest is due to UAVs' advantages unmatched by traditional ground-based networks, e.g., fast three-dimensional (3D) deployment and maneuverability.

UAVs offer several benefits, as described in [57], [58]. Their altitudes increase the likelihood of establishing LOS links with ground gNBs, resulting in more reliable data transmission compared to terrestrial networks with potential obstructions. Additionally, UAVs can adjust their positions to improve signal quality and provide dynamic deployment capabilities. They can reposition autonomously to meet real-time network needs, enhancing network robustness and adaptability to changing conditions. UAVs can be rapidly deployed in emergencies, e.g., natural disasters, without the need for site rentals or extensive setup. They can form swarms to quickly expand network coverage. However, due to battery limitations, UAVs are best suited for temporary solutions, making them ideal for events and disaster response.

UAVs can operate mainly as aerial BSs/relays or as aerial UEs. In the aerial base station/relay role, UAVs provide reliable and fast-deployable wireless communication. Conversely, UAVs functioning as aerial UEs are suited for data collection, delivery tasks, and surveillance [59].

UAVs can also be categorized by their operational altitude [56]. In this class, we can mention at least two categories: high altitude platform (HAP) and low altitude platform (LAP). HAPs operate above 20 km and remain quasi-stationary for extended periods, while LAPs fly at lower altitudes, typically up to tens of meters, and are valued for their rapid deployment and mobility [60].

Recognizing the potential of UAVs, the 3GPP has undertaken extensive studies on UAV integration. TR 22.829 [61] explores UAV support for various low altitudes applications, while TR 36.777 [62] focuses on their integration with LTE networks. Additionally,

TR 23.754 [63] and TS 23.256 [64] examine mechanisms for UAV identification, tracking, authorization, and authentication.

In the following, we present some works that focus on the synergy between UAVs and networks with wireless backhaul. Notable works in the area of UAV-IAB integration include [65], [66]. In [65], the authors examine the system-level impact of deploying UAVs with IAB on mobile UE performance. They compare static and mobile UAV-IAB setups and optimize UAV mobility using a particle swarm optimization (PSO) algorithm. Three backhaul scenarios are considered: 1) backhaul-unaware (limited bandwidth not considered in optimization); 2) backhaul-aware (limited bandwidth considered in optimization); and ideal (unlimited bandwidth). The study assesses UE throughput and Jain's fairness index for various numbers of deployed UAVs.

In [66], the authors explore a public safety scenario, where a UAV-IAB node covers an area affected by infrastructure failure. The UAV-IAB node, which operates in the mid-band frequency, receives signals from a nearby BS, offering broader coverage compared to mmWave bands. The study proposes a RL solution to optimize the UAV-IAB node's 3D positioning and antenna tilt. They also outline the required network architecture and signaling procedures for deploying their solution. System-level simulations show that their approach improves throughput and reduces UE drop rates.

To the best of our knowledge, no research has yet documented the mounting of an NCR onto a UAV. This gap indicates potential for exploring UAV-NCR technology.

The works [67], [68] investigate using RIS mounted on UAVs to enhance wireless communication. In [67], a method is proposed for optimizing the RIS phase vector and bandwidth allocation for each UE using long short-term memory (LSTM) and federated learning. This two-stage approach involves the UAV first training a model to predict the phase vector and then using the RIS to maximize the total achievable data rate.

In [68], the authors propose a model combining Q-learning and Fourier feature mapping for a RIS-mounted UAV system. This model optimizes UAV-RIS positioning, transmission beamforming, and RIS reflection beamforming. The goal is to enhance communication quality of service (QoS), reliability, and security against eavesdroppers and jammers.

### III. SYSTEM MODEL

Based on use case 5.11.2.2 "User outside the vehicle" of [69], a scenario is considered where an outdoor event takes place, i.e., a bike race. As shown in Fig. 5, a simplified Madrid grid scenario [70] is considered. Cameramen on motorcycles broadcast live videos of the race. Half of them are positioned on one street and the other, on a parallel street.

In this scenario, six different deployments are considered. The first deployment includes only two traditional macro gNBs (black nodes in Fig. 5). The second, third, and fourth deployments respectively add stationary IAB nodes, stationary NCRs, or stationary RISs to the traditional macro gNBs (with IAB and NCR represented by blue nodes and RIS by yellow nodes in Fig. 5). The RIS is strategically placed at a different position to take advantage of its reflective properties. The fifth

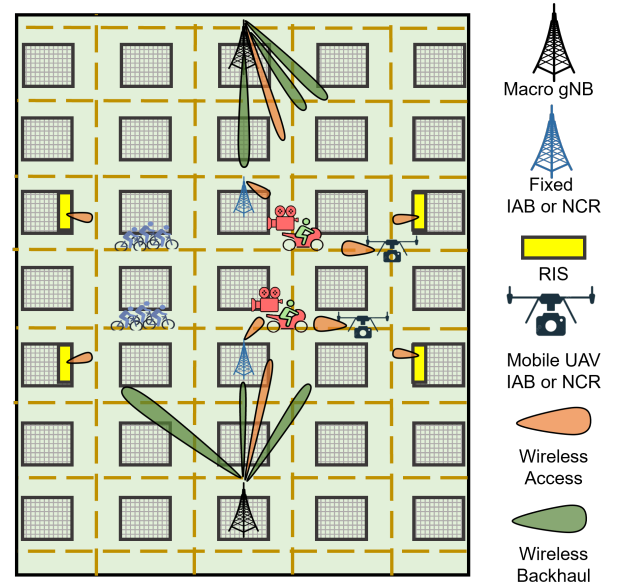


Fig. 5: Illustration of the possible deployments to serve the cameramen on motorcycles: only gNBs, stationary IAB/NCR/RIS, and UAV mounted IAB/NCR nodes.

and sixth scenarios consider the deployment of IAB nodes or NCRs mounted on mobile UAVs to follow the cameramen, in addition to the traditional macro gNBs.

In the second and third deployments, the stationary IAB node and NCR are positioned two blocks away from the gNB, as shown in Fig. 5. Both nodes are equipped with three antenna arrays each for improved street coverage. These arrays are spaced  $120^\circ$  apart to reduce interference. One array, referred to as the backhaul antenna array, faces the gNB, while the other two, known as access antenna arrays, are directed towards the street where the cameramen are located, with  $120^\circ$  between them. In contrast, the mobile UAV is equipped with only two antenna arrays to minimize weight: one for the backhaul link and one for the access links.

In the fourth deployment, the RISs are positioned differently from the stationary IAB nodes and NCRs due to their reflection properties. Four RISs are used instead of two to enhance coverage and match the number of access antenna arrays of the stationary IAB nodes and NCRs.

The following subsections present the signal to interference-plus-noise ratio (SINR) expressions for UEs connected via an IAB node, NCR, or RIS. These equations are formulated for the DL, though a similar approach applies to the UL. Additionally, IAB operates in in-band mode. The available frequency band is divided into  $K$  physical resource blocks (PRBs), where each PRB consists of a number of adjacent subcarriers.

#### A. SINR of UEs Served by IAB Nodes

The useful power  $S_{u_x,k}^{IAB}$  received by UE  $u_x$  served by an IAB node, e.g., IAB node  $r_x$ , at PRB  $k$  can be expressed as:

$$S_{u_x,k}^{IAB} = \gamma_{r_x,u_x,k} \cdot p_{r_x,u_x,k}, \quad (1)$$

where  $p_{r_x, u_x, k}$  is transmit power used by IAB node  $r_x$  to transmit useful signal to UE  $u_x$  at PRB  $k$ ; and  $\gamma_{i, j, k} = \mathbf{d}_{j, k} \mathbf{H}_{i, j, k} \mathbf{f}_{i, k}$  denotes the combined effect of the channel  $\mathbf{H}_{i, j, k}$  after the transmission and reception filters  $\mathbf{f}_{i, k}$  and  $\mathbf{d}_{j, k}$ , respectively, applied to a signal transmitted by node  $i$  to node  $j$  at PRB  $k$ .

The interference signals on UE  $u_x$  comes from two types of sources: backhaul links and access links. More precisely, signals belonging to the first type are transmitted at PRB  $k$  by a given IAB node, e.g., IAB node  $r_i$ , to its serving gNB  $b_i$ . Moreover, signals belonging to the second type are transmitted in the access links for other UEs, e.g., UE  $u_y$ , at PRB  $k$ . The transmitter  $q_y$  is its serving node, which can be either another IAB or a macro gNB. Thus, the interference  $I_{u_x, k}^{IAB}$  perceived by UE  $u_x$  at PRB  $k$  is equal to:

$$I_{u_x, k}^{IAB} = \sum_{(r_i, b_i) \in \mathcal{R} \times \mathcal{B}} \gamma_{r_i, u_x, k} \cdot p_{r_i, b_i, k} + \sum_{\substack{(q_y, u_y) \in (\mathcal{R} \cup \mathcal{B}) \times \mathcal{U}, \\ y \neq x}} \gamma_{q_y, u_x, k} \cdot p_{q_y, u_y, k}, \quad (2)$$

where  $\mathcal{R}$ ,  $\mathcal{B}$  and  $\mathcal{U}$  are the sets of IABs nodes, gNBs and UEs in the system, respectively.

Finally, the SINR  $\rho_{u_x, k}^{IAB}$  perceived by UE  $u_x$  at PRB  $k$  is

$$\rho_{u_x, k}^{IAB} = \frac{S_{u_x, k}^{IAB}}{I_{u_x, k}^{IAB} + \sigma_k^2}, \quad (3)$$

where  $\sigma_k^2$  is the noise component at PRB  $k$ .

### B. SINR of UEs Served through NCRs

It is neither considered the link between NCRs nor the NCR self-interference. The former can be mitigated during the deployment by avoiding overlapping coverage areas. The latter can be mitigated by placing the NCR antenna arrays at an angular distance of 120 degrees or more [37].

Consider a UE  $u_x$  connected to gNB  $b_x$  through NCR  $s_x$ . Its useful power received at PRB  $k$  can be split into two parts, i.e., the gNB direct link and the link through the NCR:

$$S_{u_x, k}^{NCR} = \gamma_{b_x, u_x, k} \cdot p_{b_x, u_x, k} + \gamma_{s_x, u_x, k} \cdot g_{s_x, k} \cdot \gamma_{b_x, s_x, k} \cdot p_{b_x, u_x, k}, \quad (4)$$

where  $p_{b_x, u_x, k}$  is the power transmitted by gNB  $b_x$ , and  $g_{s_x, k}$  is the stationary power gain applied by NCR  $s_x$  at PRB  $k$ .

The interference can be split into three sets: 1) signals received directly from other gNBs, e.g., gNB  $b_i$  with  $i \neq x$ , and transmitted at PRB  $k$  to others UEs  $u_y$ ; 2) copies of the signals that belong to the first set and that were amplified by an NCR; and 3) amplified noises from all NCRs with exception of the one UE  $u_x$  is connected through. Thus, the interference  $I_{u_x, k}^{NCR}$  perceived by UE  $u_x$  at PRB  $k$  is equal to:

$$I_{u_x, k}^{NCR} = \sum_{\substack{(u_y, b_y) \in \mathcal{U} \times \mathcal{B}, \\ y \neq x}} \gamma_{b_y, u_x, k} \cdot p_{b_y, u_y, k} + \sum_{\substack{(u_y, b_y) \in \mathcal{U} \times \mathcal{B}, \\ y \neq x}} \sum_{s_i \in \mathcal{S}} \gamma_{s_i, u_x, k} \cdot g_{s_i, k} \cdot \gamma_{b_y, s_i, k} \cdot p_{b_y, u_y, k} + \sigma_k^2 \cdot \sum_{\substack{s_i \in \mathcal{S}, \\ y \neq x}} \gamma_{s_i, u_x, k} \cdot g_{s_i, k}, \quad (5)$$

where  $\mathcal{S}$  is the set of NCRs.

The overall noise power  $N_{u_x, k}$  received by UE  $u_x$  at PRB  $k$  is the noise component plus the noise amplified by the NCR to which UE  $u_x$  is connected to. It can be expressed as:

$$N_{u_x, k} = \sigma_k^2 (1 + \gamma_{s_x, u_x, k} \cdot g_{s_x, k}). \quad (6)$$

Finally, the SINR  $\rho_{u_x, k}^{NCR}$  perceived by UE  $u_x$  at PRB  $k$  is

$$\rho_{u_x, k}^{NCR} = \frac{S_{u_x, k}^{NCR}}{I_{u_x, k}^{NCR} + N_{u_x, k}}. \quad (7)$$

### C. SINR of UEs Served through RISs

Consider a UE  $u_x$  connected to gNB  $b_x$  through RIS  $t_x$ . The useful power  $S_{u_x, k}^{RIS}$  received at PRB  $k$  by UE  $u_x$  can be split into two parts as in the NCR case, i.e., the direct link from the gNB and the link through the RIS:

$$S_{u_x, k}^{RIS} = \gamma_{b_x, u_x, k} \cdot p_{b_x, u_x, k} + \eta_{b_x, u_x, k} \cdot p_{b_x, u_x, k}, \quad (8)$$

where  $\eta_{i, j, k} = \mathbf{d}_{j, k} \mathbf{H}_{t_x, j, k} \mathbf{\Theta} \mathbf{H}_{i, t_x, k} \mathbf{f}_{i, k}$  denotes the combined effect of the channel when signal is received through RIS.  $\mathbf{H}_{i, t_x, k}$  is the channel between transmitter  $i$ , whose precoder is  $\mathbf{f}_{i, k}$ , and the RIS  $t_x$  at PRB  $k$ . The matrix of reflection coefficients is given by  $\mathbf{\Theta}$  and its calculation is based on [51], which is an algorithm optimizes the reflection coefficients and gNB beamforming for maximizing the signal strength received by the UE.  $\mathbf{H}_{t_x, j, k}$  is channel between RIS  $t_x$  and receiver  $j$ , whose combiner is  $\mathbf{d}_{j, k}$  at PRB  $k$ .

As in the NCR case, we neither consider the RIS self-interference nor interference between RISs. In practice, RIS depends on LOS link in outdoor urban settings, where the likelihood of RIS-RIS links is minimal due to obstacles.

Similarly to (5), except for the third term representing amplified noise, the interference received by UE  $u_x$  is:

$$I_{u_x, k}^{RIS} = \sum_{\substack{(u_y, b_y) \in \mathcal{U} \times \mathcal{B}, \\ y \neq x}} \gamma_{b_y, u_x, k} \cdot p_{b_y, u_y, k} + \sum_{\substack{(u_y, b_y) \in \mathcal{U} \times \mathcal{B}, \\ y \neq x}} \sum_{t_i \in \mathcal{T}} \eta_{b_y, u_x, k} \cdot p_{b_y, u_y, k}, \quad (9)$$

where  $\mathcal{T}$  is the set of RISs.

Finally, the SINR  $\rho_{u_x, k}^{RIS}$  perceived by UE  $u_x$  at PRB  $k$  is

$$\rho_{u_x,k}^{RIS} = \frac{S_{u_x,k}^{RIS}}{I_{u_x,k}^{RIS} + \sigma_k^2}, \quad (10)$$

where the  $\sigma_k^2$  is the noise component at PRB  $k$ .

#### IV. PERFORMANCE EVALUATION

This section compares the performance of a scenario with only macro cells (referred to as the macro only scenario) against scenarios that include either stationary or mobile nodes (mounted on a UAV) with IAB, NCR, or RIS. Details on the used parameters are provided in Section IV-A, and the results are discussed in Section IV-B.

##### A. Simulation Assumptions

As presented in Section III, it was considered a simplified Madrid grid (Fig. 5) consisting of  $120 \text{ m} \times 120 \text{ m}$  blocks with 3 m wide sidewalks and 14 m wide streets. The UEs, i.e., cameramen's equipments, were initially placed in the left block, with half in the upper middle street and the other half in the lower middle street, as depicted in Fig. 5. Additionally, the UEs moved through 3 blocks at a speed of 40 km/h.

The adopted channel model was based on the 3GPP standards outlined in [72] and [62]. It featured a carrier frequency of 28 GHz with bandwidth of 50 MHz. The model accounted for spatial and temporal consistency, distance-dependent path loss, lognormal shadowing, and small-scale fading. Details of our channel model implementation are provided in [73]. Other channel characteristics are listed in Tables II and III.

In the time domain, the minimum scheduling unit was a slot of 0.25 ms with 14 orthogonal frequency division multiplexing (OFDM) symbols. The considered TDD scheme alternated DL and UL transmissions between slots. Regarding the frequency domain, one PRB consisted of 12 consecutive subcarriers with subcarrier distance of 60 kHz. The PRB allocation was based on the round robin (RR) scheduler.

Concerning the link adaptation, a target block error rate (BLER) of 10% was set using the channel quality indicator (CQI)/modulation and coding scheme (MCS) mapping curves standardized in [74]. An outer loop strategy was considered to avoid the increase of the BLER. It decreased the estimated SINR by 1 dB after transmission errors and increased by 0.1 dB after error-free transmissions. Tables I and III present other simulation parameters.

##### B. Simulation Results

Figures 6 and 7 present the cumulative distribution function (CDF) of the SINR in DL and UL, respectively, as detailed in Eqs. (3), (7) and (10) for IAB, NCR and RIS, respectively. In the baseline scenario, i.e., the macro only scenario (dotted green curves), the UEs experienced lower SINR, particularly in the UL, with 80% of UEs connections having SINR below 2.6 dB. This was due to low UE transmit power and the distance between gNB and UEs, i.e., exceeding 300 m. This highlights the need of improving UL links. Furthermore, we can see that deploying IAB nodes and NCRs as either

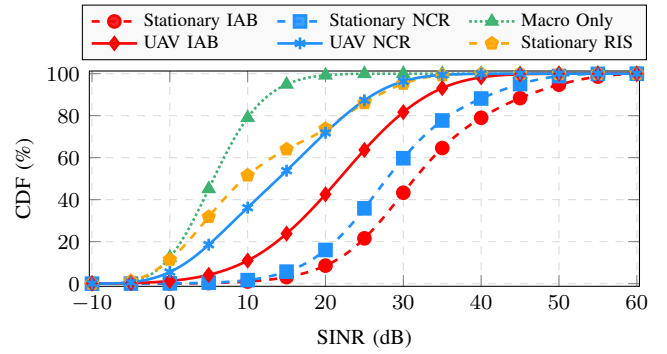


Fig. 6: CDF of SINR in DL.

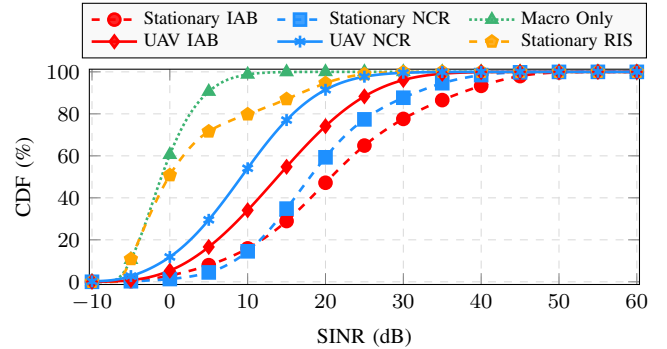


Fig. 7: CDF of SINR in UL.

stationary or mounted on mobile UAVs and RIS improved the SINR of the UEs in both UL and DL compared to macro only.

In scenarios with stationary nodes (dashed curves), IAB performed better than NCR, and NCR outperformed RIS. This is because the SINR for NCR accounts for backhaul link quality (Eq. (7)), while IAB does not (Eq. (3)). In the results shown, NCR benefited from a LOS backhaul link (Table II). Performance differences between stationary NCR and IAB are more pronounced with non-line of sight (NLOS) backhaul, as will be discussed later. This underscores the importance of a LOS backhaul for NCR deployments.

In the UL (Fig. 7), UEs with lower SINR experienced slightly better SINR with NCR compared to IAB. This is because IAB introduces interference in UE UL transmissions due to its backhaul simultaneously operating in DL, unlike NCR, where both backhaul and access links operated in UL.

Comparing NCR and RIS, unlike NCR, the RIS did not amplify the SINR, it merely reflected the signal. This underscores the importance of LOS propagation for RIS to deliver beneficial outcomes.

In the RIS scenario, the lower part of the SINR curves resembles the macro-only case, while the higher part shows improved SINR values. This is because the RIS was optimized to point towards a specific UE, benefiting its neighbors but not others farther. Thus, UEs not within the RIS optimization range communicated directly with the macro BS, leading to similar low SINR values as the macro-only scenario.

Comparing the scenarios with IAB and NCR mounted on a UAV, IAB performed better than NCR in both DL and UL. Although the NCR was expected to benefit from LOS backhaul, this did not compensate for its lower performance.

TABLE I: Entities characteristics.

Parameter	Macro gNB	Stationary IAB/NCR	Stationary RIS	UAV IAB/NCR	UE
Height	25 m	10 m	40 m	40 m	1.5 m
Transmit power	35 dBm	32 dBm	-	29 dBm	24 dBm
Antenna array	URA 8 × 8	URA 4 × 4 (3 panels)	URA 8 × 8	URA 4 × 4 (2 panels)	Single Antenna
Antenna elem. pattern	3GPP 3D [71]	3GPP 3D [71]	3GPP 3D [71]	3GPP 3D [71]	Omni
Max. antenna elem. gain	8 dBi	8 dBi	8 dBi	8 dBi	0 dBi
Speed	0 km/h	0 km/h	0 km/h	40 km/h	40 km/h

TABLE II: Characteristics of the links in same cell.

Link in same cell	Scenario	LOS/NLOS
gNB - UE	Urban Macro [72]	NLOS
gNB - Stationary IAB/NCR/RIS	Urban Macro [72][62]	LOS
gNB - Mobile UAV w/ IAB/NCR	Urban Macro [62]	LOS
IAB/NCR/RIS - UE	Urban Micro [72][62]	LOS
Mobile UAV w/ IAB/NCR - UE	Urban Micro [62]	LOS
UE - UE	Urban Micro [72]	LOS
Link in different cell	Scenario	LOS/NLOS
gNB - UE	Urban Macro [72]	NLOS
gNB - Stationary IAB/NCR/RIS	Urban Macro [72][62]	NLOS
gNB - Mobile UAV w/ IAB/NCR	Urban Macro [62]	LOS
IAB/NCR/RIS - UE	Urban Micro [72][62]	NLOS
Mobile UAV w/ IAB/NCR - UE	Urban Micro [62]	LOS
UE - UE	Urban Micro [72]	NLOS

TABLE III: Simulation parameters.

Parameter	Value
Carrier frequency	28 GHz
System bandwidth	50 MHz
Subcarrier spacing	60 kHz
Number of subcarriers per PRB	12
Number of PRBs	66
Slot duration	0.25 ms
OFDM symbols per slot	14
Channel generation procedure	As described in [71, Fig.7.6.4-1]
Path loss	Eqs. in [71, Table 7.4.1-1]
Fast fading	As described in [71, Sec.7.5] and [71, Table 7.5-6]
AWGN density power per subcarrier	-174 dBm/Hz
Noise figure	9 dB
Number of UEs	8
Traffic model	Full buffer
NCR gain	60 dB

Stationary nodes consistently achieved higher SINR values compared to mobile UAV nodes. In DL, this was due to stationary nodes having twice the transmit power of UAV nodes. In UL, stationary nodes benefited from shorter distances to UEs. Additionally, stationary nodes had double the number of access panels compared to mobile UAV nodes, which only had one access panel. These constraints in UAVs' transmit power and number of access panels are related to the UAVs' capability and size limitations compared to stationary nodes.

Figures 8 and 9 present the CDF of the UEs' throughput in DL and UL, respectively. The throughput analysis reveals similar conclusions to the SINR results. The macro-only scenario, as a baseline, showed lower throughput values, especially in UL, where 80% of UE connections had throughput below 5 Mbps. Compared to the macro-only scenario, UE throughput was higher with IAB, NCR, and RIS.

Comparing stationary IAB and stationary NCR, UEs with high throughput benefited more from NCR due to the TDD scheme and HD mode of IAB. In the IAB case, a UE required at least 2 transmission time intervals (TTIs) to receive a packet,

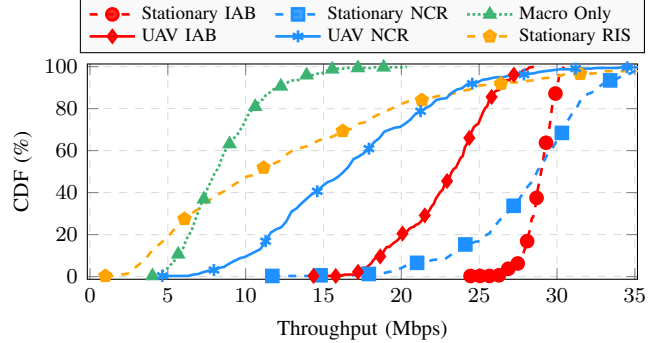


Fig. 8: CDF of throughput in DL.

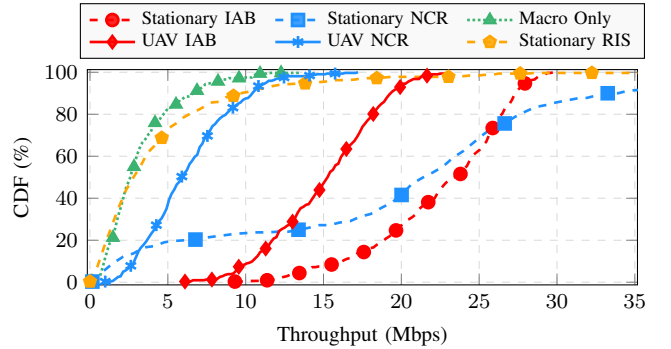


Fig. 9: CDF of throughput in UL.

whereas with NCR, only 1 TTI was needed. Conversely, UEs with low throughput performed better with IAB nodes. This is because, with IAB, backhaul and access links are independent, whereas NCR requires successful transmission on both links simultaneously, increasing the likelihood of retransmissions with a poor backhaul or forward link.

In terms of throughput, UEs with low throughput saw greater improvements in DL, while UEs with high throughput experienced higher gains in UL from the presence of assisting nodes. Specifically, compared to the macro-only scenario, at the 10<sup>th</sup> percentile, IAB provided gains of 22.12 Mbps (+397.67%) in DL and 15.32 Mbps (1,859.76%) in UL. For the NCR, they were 17.45 Mbps (317.02%) in DL and 0.87 Mbps (114.63%) in UL. At the 90<sup>th</sup> percentile, they were 18.05 Mbps (149.50%) and 20.86 Mbps (312.42%), for the IAB in DL and IAB in UL, respectively, and 20.76 Mbps (172.08%) and 27.17 Mbps (411.36%) for the NCR in DL and NCR in UL, respectively. This variation is due to DL signals being stronger at the cell edges with IAB/NCR, and UL signals benefiting from shorter distances to the nodes, avoiding bottlenecks caused by low transmit power.

Regarding RIS throughput, the RIS generally improved throughput for most UEs, despite not amplifying reflected

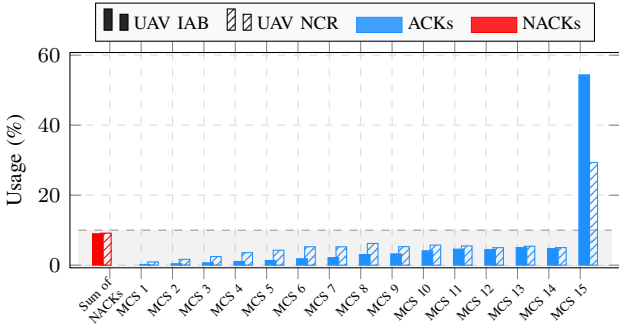


Fig. 10: MCS of UAV IAB in UL.

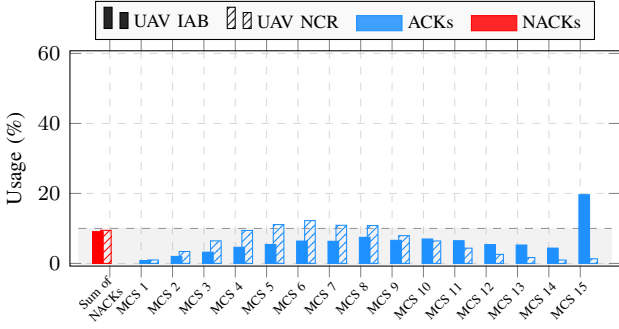


Fig. 11: MCS of UAV NCR in UL.

signals. It provided an alternative path between the gNB and UE, helping signals bypass obstacles in the LOS path. However, some UEs experienced worse throughput with RIS compared to the macro-only scenario. This issue arose because, as already presented, the RIS optimized performance for a specific cluster of UEs, and gNB might have overestimated the SINR for UEs less well covered by the RIS beam, leading to failed transmissions and retries with adjusted SINR estimates.

In the UAV scenarios, UAV IAB outperformed UAV NCR in throughput. Compared to stationary nodes, the transmit power and gain of UAV NCR were insufficient to achieve high SINR, leading UAV NCR to use lower MCSs than UAV IAB in both directions. This is illustrated in Figures 10 and 11, which show the MCS and the percentage of acknowledgements (ACKs) and no acknowledgements (NACKs) for UAV IAB and UAV NCR in DL and UL, respectively. ACK and NACK indicate successful and failed transmissions, respectively. The UAV IAB had more transmission in the MCS 15 than the UAV NCR in both directions. Whereas, in DL, the MCS of UAV NCR was more concentrated in the MCS 15, in UL, its MCS was spread to lower values.

Finally, Figures 12 and 13 present the Jain's fairness index in terms of UEs' throughput in DL and UL, respectively. The Jain's fairness index, i.e.,  $\Delta = (\sum_{u \in \mathcal{U}} \theta_u)^2 / (|\mathcal{U}| \sum_{u \in \mathcal{U}} (\theta_u)^2)$  with  $\theta_u$  being the throughput of UE  $u$ , is defined as the ratio between the square of the sum of all UEs' throughputs and the product between the number of UEs and the sum of the squares of each UEs' throughput [75]. RIS had the lowest fairness between the UEs. This is due to the fact that RIS implementation benefited just a set of UEs to which the signal reflected by RIS highly improved the UEs' SINR, while, the

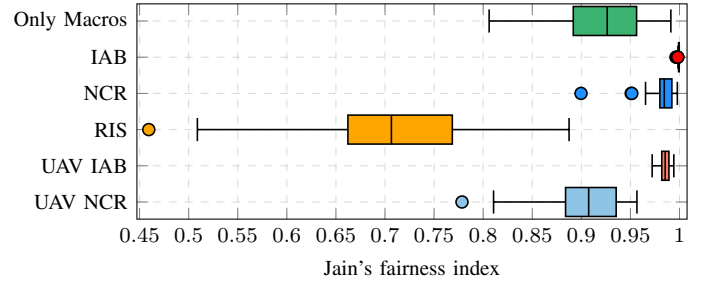


Fig. 12: Jain's fairness index in DL.

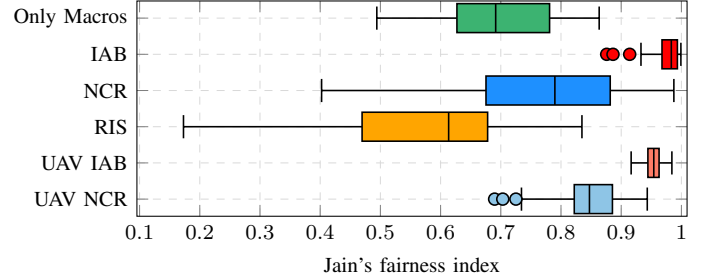


Fig. 13: Jain's fairness index in UL.

other UEs in the system continued with low SINR being served by the gNB. In the IAB case, as explained before, UEs with high SINR gain had their gain in terms of throughput limited by the TDD schemes and HD mode (at least 2 TTIs to execute a transmission). This made the system fairer, by avoiding some UEs to have a really high throughput gain.

## V. CONCLUSIONS

In light of the growing need for network densification, IAB, NCR, and RIS are alternative technologies to assist the gNBs. These nodes can be more cost-effective and quicker to deploy than wired backhaul solutions. In this context, the present work overviewed their main characteristics also providing their main investigated topics. Moreover, their performances were analyzed in the context of an outdoor sport event. The study compared stationary deployments of IAB, NCR, and RIS, as well as mobile IAB and NCR mounted on UAVs. The analyses concluded that both stationary and mobile (UAV-mounted) IAB and NCR deployments are effective for extending coverage to cell-edge and obstructed areas. Also, both IAB and NCR outperform the RIS, in terms of throughput and UE's experienced SINR. They also improve the UEs UL transmissions, which can be a bottleneck in traditional networks. Moreover, these solutions also facilitate the rapid deployment of new cells, enhancing connectivity in high-demanding areas. Furthermore, UAV-mounted nodes have proven to be useful in scenarios where LOS links for stationary deployments are obstructed. However, successful implementation of these technologies requires careful network planning and environment-specific topology design.

## REFERENCES

- [1] Ericsson. "Mobile data traffic outlook." (), [Online]. Available: <https://www.ericsson.com/en/reports-and-papers/mobility-report/dataforecasts/mobile-traffic-forecast> (visited on 05/10/2024).

- [2] 3GPP, “NR; NR and NG-RAN Overall description; Stage 2,” 3rd Generation Partnership Project (3GPP), TS 38.300, Dec. 2019, v.15.8.0. [Online]. Available: <http://www.3gpp.org/ftp/Specs/html-info/38300.htm> (visited on 02/17/2020).
- [3] R. Flamini, D. De Donno, J. Gambini, *et al.*, “Towards a heterogeneous smart electromagnetic environment for millimeter-wave communications: An industrial viewpoint,” *IEEE Trans. Antennas Propag.*, vol. 70, no. 10, pp. 8898–8910, Feb. 2022. DOI: 10.1109/TAP.2022.3151978.
- [4] S. Rangan, T. S. Rappaport, and E. Erkip, “Millimeter-wave cellular wireless networks: Potentials and challenges,” *Proc. IEEE*, vol. 102, no. 3, pp. 366–385, 2014. DOI: 10.1109/JPROC.2014.2299397.
- [5] R. A. Ayoubi, M. Mizmizi, D. Tagliaferri, D. D. Donno, and U. Spagnolini. “Network-controlled repeaters vs. reconfigurable intelligent surfaces for 6G mmW coverage extension.” arXiv: 2211.08033. (Nov. 2022).
- [6] V. F. Monteiro, F. R. M. Lima, D. C. Moreira, *et al.*, “Paving the way towards mobile IAB: Problems, solutions and challenges,” *IEEE Open J. Commu. Soc.*, vol. 3, pp. 2347–2379, Nov. 2022. DOI: 10.1109/OJCOMS.2022.3224576.
- [7] 3GPP, “Overview of 3GPP release 10,” 3rd Generation Partnership Project (3GPP), Tech. Rep., Jun. 2014, v.0.2.1. [Online]. Available: [https://www.3gpp.org/ftp/Information/WORK\\_PLAN/Description\\_Releases/Rel-10\\_description\\_20140630.zip](https://www.3gpp.org/ftp/Information/WORK_PLAN/Description_Releases/Rel-10_description_20140630.zip).
- [8] M. Jaber, M. A. Imran, R. Tafazolli, and A. Tukmanov, “5G backhaul challenges and emerging research directions: A survey,” *IEEE Access*, vol. 4, pp. 1743–1766, 2016.
- [9] C. B. Czegledi, M. Hörberg, M. Sjödin, *et al.*, “Demonstrating 139 gbps and 55.6 bps/hz spectrum efficiency using 8x8 mimo over a 1.5-km link at 73.5 ghz,” in *Proc. of the IEEE MTT-S Internat. Microw. Symp. (IMS)*, 2020, pp. 539–542.
- [10] B. Tezergil and E. Onur, “Wireless backhaul in 5G and beyond: Issues, challenges and opportunities,” *IEEE Commun. Surveys Tuts.*, vol. 24, no. 4, pp. 2579–2632, 2022.
- [11] 3GPP, “NR; study on integrated access and backhaul (release 16),” 3rd Generation Partnership Project (3GPP), TR 38.874, Dec. 2018, v.16.0.0. [Online]. Available: <http://www.3gpp.org/ftp/Specs/html-info/38874.htm> (visited on 04/13/2021).
- [12] 3GPP, “Study on NR network-controlled repeaters,” 3rd Generation Partnership Project (3GPP), TR 38.867, Sep. 2022, v.18.0.0. [Online]. Available: <http://www.3gpp.org/DynaReport/38867.htm>.
- [13] *Rws-210019: Nr smart repeaters*, Qualcomm, 2021.
- [14] ETSI, “Reconfigurable intelligent surfaces (RIS); use cases, deployment scenarios and requirements,” European Telecommunications Standards Institute (ETSI), GR 001, Apr. 2023, V1.1.1. [Online]. Available: [https://www.etsi.org/deliver/etsi\\_gr/RIS/001\\_099/001/01.01.01\\_60/gr\\_RIS001v010101p.pdf](https://www.etsi.org/deliver/etsi_gr/RIS/001_099/001/01.01.01_60/gr_RIS001v010101p.pdf).
- [15] M. Astrom, P. Gentner, O. Haliloglu, B. Makki, and O. Tageman. “RIS in cellular networks - challenges and issues.” arXiv: 2404.04753 [cs.NI]. (Apr. 2024).
- [16] Q. Wu, S. Zhang, B. Zheng, C. You, and R. Zhang, “Intelligent reflecting surface-aided wireless communications: A tutorial,” *IEEE Trans. Commun.*, vol. 69, no. 5, pp. 3313–3351, 2021.
- [17] C.-K. Wen, L.-S. Tsai, A. Shojaeifard, P.-K. Liao, K.-K. Wong, and C.-B. Chae, “Shaping a smarter electromagnetic landscape: IAB, NCR, and RIS in 5G standard and future 6G,” *IEEE Control Syst. Mag.*, vol. 8, no. 1, pp. 72–78, 2024.
- [18] 3GPP, “NR; integrated access and backhaul radio transmission and reception,” 3rd Generation Partnership Project (3GPP), TS 38.174, Dec. 2020, v.16.1.0. [Online]. Available: <http://www.3gpp.org/ftp/Specs/html-info/38174.htm> (visited on 04/13/2021).
- [19] 3GPP, “New WID on Enhancements to Integrated Access and Backhaul,” 3rd Generation Partnership Project (3GPP), RP 210758, Mar. 2021, Meeting no. 91e. [Online]. Available: [https://www.3gpp.org/tp/TSG\\_RAN/TSG\\_RAN/TSGR\\_91e/DocsRP-210758.zip](https://www.3gpp.org/tp/TSG_RAN/TSG_RAN/TSGR_91e/DocsRP-210758.zip) (visited on 04/18/2021).
- [20] 3GPP, “NR; Backhaul Adaptation Protocol (BAP) specification (Release 16),” 3rd Generation Partnership Project (3GPP), TS 38.340, Mar. 2021, v.16.4.0. [Online]. Available: <http://www.3gpp.org/ftp/Specs/html-info/38340.htm> (visited on 04/15/2021).
- [21] C. Madapatha, B. Makki, C. Fang, *et al.*, “On integrated access and backhaul networks: Current status and potentials,” *IEEE Open J. Commu. Soc.*, vol. 1, pp. 1374–1389, Sep. 2020. DOI: 10.1109/OJCOMS.2020.3022529.
- [22] C. Madapatha, B. Makki, A. Muhammad, E. Dahlman, M.-S. Alouini, and T. Svensson, “On topology optimization and routing in integrated access and backhaul networks: A genetic algorithm-based approach,” *IEEE Open J. Commu. Soc.*, vol. 2, pp. 2273–2291, Sep. 2021. DOI: 10.1109/OJCOMS.2021.3114669.
- [23] F. I. G. Carvalho, T. F. Maciel, R. V. de O. Paiva, and I. B. Palhano, “Genetic algorithm for base station placement in integrated access and backhaul networks,” in *Proc. of the IEEE Workshop on Commun. Networks and Power Systems (WCNPS)*, 2023, pp. 1–7.
- [24] M. Polese, M. Giordani, T. Zugno, *et al.*, “Integrated access and backhaul in 5G mmWave networks: Potential and challenges,” *IEEE Commu. Mag.*, vol. 58, no. 3, pp. 62–68, Mar. 2020. DOI: 10.1109/MCOM.001.1900346.
- [25] Q.-H. Tran, T.-M. Duong, and S. Kwon, “Load balancing for integrated access and backhaul in mmwave small cells,” *IEEE Access*, vol. 11, pp. 138 664–138 674, Dec. 2023. DOI: 10.1109/ACCESS.2023.3338567.
- [26] C. Ghodhbane, M. Manini, P. Savelli, C. Gueguen, and X. Lagrange, “Load-efficiency-balance cell selection policy for iab networks,” in *Proc. of the IEEE Personal, Indoor and Mob. Radio Commun. (PIMRC)*, 2023, pp. 1–6. DOI: 10.1109/PIMRC56721.2023.10293897.
- [27] W. Lei, Y. Ye, and M. Xiao, “Deep reinforcement learning-based spectrum allocation in integrated access and backhaul networks,” *IEEE Trans. on Cogn. Commun. Netw.*, vol. 6, no. 3, pp. 970–979, May 2020. DOI: 10.1109/TCCN.2020.2992628.
- [28] J. Y. Lai, W.-H. Wu, and Y. T. Su, “Resource allocation and node placement in multi-hop heterogeneous integrated-access-and-backhaul networks,” *IEEE Access*, vol. 8, pp. 122 937–122 958, Jul. 2020. DOI: 10.1109/ACCESS.2020.3007501.
- [29] M. Sana and B. Miscopein, “Learning hierarchical resource allocation and multi-agent coordination of 5G mobile IAB nodes,” in *Proc. of the IEEE Internat. Conf. on Commun. (ICC)*, 2023, pp. 4218–4223.
- [30] 3GPP, “NR repeaters,” 3rd Generation Partnership Project (3GPP), RP 210818, Mar. 2021, TSG-RAN meeting no. 91e. [Online]. Available: [https://www.3gpp.org/ftp/tsg\\_ran/TSG\\_RAN/TSGR\\_91e/Docs/RP-210818.zip](https://www.3gpp.org/ftp/tsg_ran/TSG_RAN/TSGR_91e/Docs/RP-210818.zip) (visited on 03/17/2022).
- [31] J. Xin, S. Xu, S. Xiong, H. Xu, and H. Zhang, “A survey on network controlled repeater technology,” in *Proc. of the IEEE Internat. Conf. on Comput. and Commun. (ICCC)*, 2022, pp. 1097–1101.
- [32] G. C. M. da Silva, D. A. Sousa, V. F. Monteiro, *et al.*, “Impact of network deployment on the performance of NCR-assisted networks,” in *Proc. of the IEEE Internat. Symposium on Wireless Commun. Syst. (ISWCS)*, 2024, pp. 1–6.
- [33] F. I. G. Carvalho, R. V. de O. Paiva, T. F. Maciel, *et al.* “Network-controlled repeater - an introduction.” arXiv: 2403.09601 [cs.NI]. (Jan. 2024).
- [34] G. Leone, E. Moro, I. Filippini, A. Capone, and D. D. Donno, “Towards reliable mmWave 6G RAN: Reconfigurable surfaces, smart repeaters, or both?” In *Proc. of the Internat. Symp. on Modeling and Opt. in Mobile, Ad Hoc, and Wireless Netw. (WiOPT)*, Turin, Italy, Sep. 2022, pp. 1–9. DOI: 10.1109/AERO.2015.7118906.
- [35] R. A. Ayoubi, M. Mizmizi, D. Tagliaferri, D. D. Donno, and U. Spagnolini, “Network-controlled repeaters vs. reconfigurable intelligent surfaces for 6G mmW coverage extension: A simulative comparison,” in *Proc. of the IEEE Mediterranean Communication and Computer Networking Conference (MedComNet)*, 2023, pp. 196–202.
- [36] H. Guo, C. Madapatha, B. Makki, *et al.* “A comparison between network-controlled repeaters and reconfigurable intelligent surfaces.” arXiv: 2211.06974 [cs.NI]. (Nov. 2022).
- [37] K. Dong, S. Mura, M. Mizmizi, D. Tagliaferri, and U. Spagnolini, “Advanced tri-sectoral multi-user millimeter-wave smart repeater,” in *Proc. of the IEEE Mediterranean Communication and Computer Networking Conference (MedComNet)*, 2023, pp. 205–210.
- [38] D. A. Sousa, F. R. M. Lima, V. F. Monteiro, T. F. Maciel, and B. Makki. “Beam squinting compensation: An NCR-assisted scenario.” arXiv: 2402.10368 [eess.SP]. (Jan. 2024).
- [39] G. C. M. da Silva, E. R. B. Falcão, V. F. Monteiro, *et al.*, “System level evaluation of network-controlled repeaters: Performance improvement of serving cell and interference impact on neighbor cells,” *Proc. of the Brazilian Telecommun. Symp. (SBRt)*, 2023. DOI: 10.14209/sbrt.2023.1570923164.
- [40] ETSI, “Reconfigurable intelligent surfaces (RIS); technological challenges, architecture and impact on standardization,” European Telecommunications Standards Institute (ETSI), GR 002, Aug. 2023, V1.1.1. [Online]. Available: [https://www.etsi.org/deliver/etsi\\_gr/RIS/001\\_099/002/01.01.01\\_60/gr\\_RIS002v010101p.pdf](https://www.etsi.org/deliver/etsi_gr/RIS/001_099/002/01.01.01_60/gr_RIS002v010101p.pdf).
- [41] ETSI, “Reconfigurable intelligent surfaces (RIS); communication models, channel models, channel estimation and evaluation methodology,” European Telecommunications Standards Institute (ETSI), GR 003, Jun. 2023, V1.1.1. [Online]. Available: [https://www.etsi.org/deliver/etsi\\_gr/RIS/001\\_099/003/01.01.01\\_60/gr\\_RIS003v010101p.pdf](https://www.etsi.org/deliver/etsi_gr/RIS/001_099/003/01.01.01_60/gr_RIS003v010101p.pdf).

- //www.etsi.org/deliver/etsi\_gr/RIS/001\_099/003/01\_01\_01\_60/gr\_RIS003v010101p.pdf.
- [42] P. R. B. Gomes, G. T. de Araújo, B. Sokal, A. L. F. de Almeida, B. Makki, and G. Fodor, "Channel estimation in ris-assisted mimo systems operating under imperfections," *IEEE Trans. Veh. Technol.*, vol. 72, no. 11, pp. 14 200–14 213, 2023.
- [43] Y. Guo, P. Sun, Z. Yuan, *et al.*, "Efficient channel estimation for RIS-aided MIMO communications with unitary approximate message passing," *IEEE Trans. Wireless Commun.*, vol. 22, no. 2, pp. 1403–1416, 2023.
- [44] A. Molazadeh, Z. Maroufi, and M. Ardebilipour, "A deep neural network-based method for mmwave time-varying channel estimation," in *Proc. of the IEEE International Conference on Information and Knowledge Technology (IKT)*, 2022, pp. 1–7.
- [45] N. Ginige, A. S. de Sena, N. H. Mahmood, N. Rajatheva, and M. Latva-aho, "Machine learning-based channel prediction for RIS-assisted MIMO systems with channel aging." arXiv: 2406.07387 [cs.LG]. (May 2024).
- [46] W. Tang, M. Z. Chen, X. Chen, *et al.*, "Wireless communications with reconfigurable intelligent surface: Path loss modeling and experimental measurement," *IEEE Trans. Wireless Commun.*, vol. 20, no. 1, pp. 421–439, 2021.
- [47] S. Meng, W. Tang, W. Chen, *et al.*, "Rank optimization for MIMO channel with RIS: Simulation and measurement," *IEEE Wireless Commun. Lett.*, vol. 13, no. 2, pp. 437–441, 2024.
- [48] Y. Chen, W. Cheng, and W. Zhang, "Reconfigurable intelligent surface equipped UAV in emergency wireless communications: A new fading-shadowing model and performance analysis," *IEEE Trans. Commun.*, vol. 72, no. 3, pp. 1821–1834, 2024.
- [49] Y. Liu and C. D. Sarris, "Efficient computation of scattered fields from reconfigurable intelligent surfaces for propagation modeling," *IEEE Trans. Antennas Propag.*, vol. 72, no. 2, pp. 1817–1826, 2024.
- [50] L. Ibrahim, M. N. Mahmud, M. F. M. Salleh, and A. Al-Rimawi, "Joint beamforming optimization design and performance evaluation of RIS-aided wireless networks: A comprehensive state-of-the-art review," *IEEE Access*, vol. 11, pp. 141 801–141 859, 2023.
- [51] M. Munawar and K. Lee, "Low-complexity adaptive selection beamforming for IRS-assisted single-user wireless networks," *IEEE Trans. Veh. Technol.*, vol. 72, no. 4, pp. 5458–5462, 2023.
- [52] H. Amirara, F. Ashtiani, M. Mirmohseni, and M. Nasiri-Kenari, "IRS-user association in IRS-aided MISO wireless networks: Convex optimization and machine learning approaches," *IEEE Trans. Veh. Technol.*, vol. 72, no. 11, pp. 14 305–14 316, 2023.
- [53] X. Mu, Y. Liu, L. Guo, J. Lin, and R. Schober, "Simultaneously transmitting and reflecting (STAR) RIS aided wireless communications," *IEEE Trans. Wireless Commun.*, vol. 21, no. 5, pp. 3083–3098, 2022.
- [54] A. R. Ndjiongue, T. M. N. Ngatched, O. A. Dobre, and H. Haas, "Re-configurable intelligent surface-based VLC receivers using tunable liquid-crystals: The concept," *J. Lightw. Technol.*, vol. 39, no. 10, pp. 3193–3200, 2021.
- [55] H. Li, S. Shen, and B. Clerckx, "Beyond diagonal reconfigurable intelligent surfaces: From transmitting and reflecting modes to single-, group-, and fully-connected architectures," *IEEE Trans. Wireless Commun.*, vol. 22, no. 4, pp. 2311–2324, 2023.
- [56] M. Mozaffari, W. Saad, M. Bennis, Y.-H. Nam, and M. Debbah, "A tutorial on uavs for wireless networks: Applications, challenges, and open problems," *IEEE Commun. Surveys Tuts.*, vol. 21, no. 3, pp. 2334–2360, 2019.
- [57] B. Li, Z. Fei, and Y. Zhang, "UAV communications for 5g and beyond: Recent advances and future trends," *IEEE Internet Things J.*, vol. 6, no. 2, pp. 2241–2263, 2019.
- [58] M. Dai, N. Huang, Y. Wu, J. Gao, and Z. Su, "Unmanned-aerial-vehicle-assisted wireless networks: Advancements, challenges, and solutions," *IEEE Internet Things J.*, vol. 10, no. 5, pp. 4117–4147, 2023.
- [59] M. K. Banafaa, Ö. Pepeoğlu, I. Shaya, *et al.*, "A comprehensive survey on 5g-and-beyond networks with uavs: Applications, emerging technologies, regulatory aspects, research trends and challenges," *IEEE Access*, vol. 12, pp. 7786–7826, 2024.
- [60] G. K. Kurt, M. G. Khoshkholgh, S. Alfattani, *et al.*, "A vision and framework for the high altitude platform station (HAPS) networks of the future," *IEEE Commun. Surveys Tuts.*, vol. 23, no. 2, pp. 729–779, 2021.
- [61] 3GPP, "Enhancement for unmanned aerial vehicles (UAVs)," 3rd Generation Partnership Project (3GPP), TR 22.829, 2018, v.17.1.0. [Online]. Available: [https://www.3gpp.org/ftp//Specs/archive/22\\_series/22.829/22829-h10.zip](https://www.3gpp.org/ftp//Specs/archive/22_series/22.829/22829-h10.zip).
- [62] 3GPP, "Enhanced LTE support for aerial vehicles," 3rd Generation Partnership Project (3GPP), TR 36.777, Jan. 2018, v.15.0.0. [Online]. Available: [https://www.3gpp.org/ftp//Specs/archive/36\\_series/36.777/36777-f00.zip](https://www.3gpp.org/ftp//Specs/archive/36_series/36.777/36777-f00.zip).
- [63] 3GPP, "Study on supporting unmanned aerial systems (UAS) connectivity, identification and tracking," 3rd Generation Partnership Project (3GPP), TR 23.754, Mar. 2021, v.17.1.0. [Online]. Available: [https://www.3gpp.org/ftp//Specs/archive/23\\_series/23.754/23754-h10.zip](https://www.3gpp.org/ftp//Specs/archive/23_series/23.754/23754-h10.zip).
- [64] 3GPP, "Support of uncrewed aerial systems (uas) connectivity, identification and tracking; stage 2," 3rd Generation Partnership Project (3GPP), TS 23.256, Dec. 2023, v.17.6.0. [Online]. Available: [https://www.3gpp.org/ftp//Specs/archive/23\\_series/23.256/23256-i20.zip](https://www.3gpp.org/ftp//Specs/archive/23_series/23.256/23256-i20.zip).
- [65] N. Tafintsev, D. Moltchanov, M. Gerasimenko, *et al.*, "Aerial access and backhaul in mmWave B5G systems: Performance dynamics and optimization," *IEEE Commun. Mag.*, vol. 58, no. 2, pp. 93–99, Feb. 2020. DOI: 10.1109/MCOM.001.1900318.
- [66] H. Zhang, J. Li, Z. Qi, *et al.*, "Autonomous navigation and configuration of integrated access backhauling for UAV base station using reinforcement learning," in *Proc. of the IEEE Future Networks World Forum (FNWF)*, 2022, pp. 184–189.
- [67] H. Park, T.-H. Nguyen, and L. Park, "Federated deep learning for RIS-assisted UAV-enabled wireless communications," in *Proc. of the Internat. Conf. on ICT Convergence (ICTC)*, 2022, pp. 831–833.
- [68] H. Yang, S. Liu, L. Xiao, Y. Zhang, Z. Xiong, and W. Zhuang, "Learning-based reliable and secure transmission for UAV-RIS-assisted communication systems," *IEEE Trans. Wireless Commun.*, pp. 1–1, 2023.
- [69] 3GPP, "Study on vehicle-mounted relays; stage 1 (release 18)," 3rd Generation Partnership Project (3GPP), TR 22.839, Sep. 2021, v.18.0.0. [Online]. Available: <http://www.3gpp.org/ftp//Specs/html-info/22839.htm> (visited on 10/20/2021).
- [70] P. Agyapong *et al.*, "Simulation guidelines," METIS, Deliverable 6.1, Oct. 2013. [Online]. Available: [https://metis2020.com/wp-content/uploads/deliverables/METIS\\_D6.1\\_v1.pdf](https://metis2020.com/wp-content/uploads/deliverables/METIS_D6.1_v1.pdf) (visited on 09/20/2021).
- [71] 3GPP, "Study on channel model for frequencies from 0.5 to 100 GHz," 3rd Generation Partnership Project (3GPP), TR 38.901, Sep. 2017, v.14.2.0. [Online]. Available: <http://www.3gpp.org/DynaReport/38901.htm> (visited on 09/26/2017).
- [72] 3GPP, "Study on channel model for frequencies from 0.5 to 100 GHz," 3rd Generation Partnership Project (3GPP), TR 38.901, Mar. 2022, v.17.0.0. [Online]. Available: <http://www.3gpp.org/DynaReport/38901.htm> (visited on 09/26/2017).
- [73] A. M. Pessoa, I. M. Guerreiro, C. F. M. e Silva, *et al.*, "A stochastic channel model with dual mobility for 5G massive networks," *IEEE Access*, vol. 7, pp. 149 971–149 987, Oct. 2019, ISSN: 2169-3536. DOI: 10.1109/ACCESS.2019.2947407.
- [74] 3GPP, "NR; physical layer procedures for data," 3rd Generation Partnership Project (3GPP), TS 38.214, Dec. 2017, v.15.0.0. [Online]. Available: <http://www.3gpp.org/ftp//Specs/html-info/38214.htm>.
- [75] R. Jain, D.-M. Chiu, and W. Hawe, "A quantitative measure of fairness and discrimination for resource allocation in shared computer systems." arXiv: cs/9809099 [cs.NI]. (Sep. 1998).